Received: 9 September 2017 | Revised: 24 October 2017 | Accepted: 28 October 2017

DOI: 10.1111/chd.12556

ORIGINAL ARTICLE

WILEY Congenital Heart Disease

Computational simulation of postoperative pulmonary flow distribution in Alagille patients with peripheral pulmonary artery stenosis

Weiguang Yang PhD[1] | Frank L. Hanley MD[2] | Frandics P. Chan PhD, MD[3] | Alison L. Marsden PhD[1,4] | Irene E. Vignon-Clementel PhD[5] | Jeffrey A. Feinstein MD[1,4]

[1]Department of Pediatrics (Cardiology), Stanford University School of Medicine, Stanford, California, USA

[2]Department of Cardiothoracic Surgery, Stanford University School of Medicine, Stanford, California, USA

[3]Department of Radiology, Stanford University School of Medicine, Stanford, California, USA

[4]Department of BioEngineering, Stanford University School of Medicine, Stanford, California, USA

[5]INRIA and Sorbonne Universités UPMC, Univ. Paris 6, Laboratoire Jacques-Louis Lions, Paris, France

Correspondence
Weiguang Yang, Research Associate, Division of Pediatric Cardiology, Stanford University School of Medicine, 750 Welch Rd, Suite 325, Palo Alto, CA 94304.
Email: wgyang@stanford.edu

Funding information
The Vera Moulton Wall Center for Pulmonary Vascular Disease at Stanford and France-Stanford Center for Interdisciplinary Studies.

Abstract

Background: Up to 90% of individuals with Alagille syndrome have congenital heart diseases. Peripheral pulmonary artery stenosis (PPS), resulting in right ventricular hypertension and pulmonary flow disparity, is one of the most common abnormalities, yet the hemodynamic effects are ill-defined, and optimal patient management and treatment strategies are not well established. The purpose of this pilot study is to use recently refined computational simulation in the setting of multiple surgical strategies, to examine the influence of pulmonary artery reconstruction on hemodynamics in this population.

Materials and Methods: Based on computed tomography angiography and cardiac catheterization data, preoperative pulmonary artery models were constructed for 4 patients with Alagille syndrome with PPS (all male, age range: 0.6–2.9 years), and flow simulations with deformable walls were performed. Surgeon directed virtual surgery, mimicking the surgical procedure, was then performed to derive postoperative models. Postoperative simulation-derived hemodynamics and blood flow distribution were then compared with the clinical results.

Results: Simulations confirmed substantial resistance, resulting from preoperative severe ostial stenoses, and the use of newly developed adaptive outflow boundary conditions led to excellent agreement with in vivo measurements. Relief of PPS decreased pulmonary artery pressures and improved pulmonary flow distribution both in vivo and in silico with good correlation.

Conclusions: Using adaptive outflow boundary conditions, computational simulations can estimate postoperative overall pulmonary flow distribution in patients with Alagille syndrome after pulmonary artery reconstruction. Obstruction relief along with pulmonary artery vasodilation determines postoperative pulmonary flow distribution and newer methods can incorporate these physiologic changes. Evolving blood flow simulations may be useful in surgical or transcatheter planning and in understanding the complex interplay among various obstructions in patients with peripheral pulmonary stenosis.

KEYWORDS

Alagille syndrome (ALGS), blood flow simulation, peripheral pulmonary artery stenosis (PPS), pulmonary adaptation and remodeling, pulmonary flow, virtual surgery

Abbreviations: CFD, computational fluid dynamics; LPA, left pulmonary artery; LPS, lung perfusion scan; MPA, main pulmonary artery; PA, pulmonary artery; PPS, peripheral pulmonary artery stenosis; RPA, right pulmonary artery; RV, right ventricular; WSS, wall shear stress.

 © 2017 Wiley Periodicals, Inc.

1 | INTRODUCTION

Alagille syndrome, with manifestations in multiple organs including liver, heart, kidney, skeletal, and nervous systems, is a rare and complex genetic disorder, resulting from mutations in JAG1 or NOTCH2.[1,2] Up to 90% of individuals with Alagille syndrome have congenital heart diseases.[1] Peripheral pulmonary artery stenosis (PPS), one of the most common cardiac malformations, can result in right ventricular (RV) hypertension, RV hypertrophy, and eventually ventricular failure.[1–4] Pulmonary artery (PA) stenoses reduce perfusion to the affected segments, and may impair downstream vessel growth. In addition, failure to restore reasonable relative pulmonary blood flow in a timely fashion may result in irreversible PA growth impairment and pulmonary blood flow maldistribution. Owing to congenital abnormalities, up to 25% of patients with Alagille syndrome may develop liver failure requiring liver transplantation, and the elevated RV pressures associated with PPS increase the risk of transplantation.[5–7] Treatment of significant pulmonary artery stenoses and the resulting reduction in the RV pressures improve both the long-term cardiac performance and the liver transplant outcomes.

Catheter-based angioplasty and/or stenting as well as surgical patch-plasties have been used to treat PPS in these patients.[8] Catheter-based interventions have been shown to be safe and cost-effective and are the treatment option chosen by most centers[4,8,9] as a surgical approach to distal PA targets can be quite difficult. Freedom from reintervention at 5 years, however, is only 22% after the first catheter-based intervention.[4] In addition, balloon dilation often leads to only fair improvements in the most severe cases, and the abnormal pulmonary tissue is at moderate risk of rupture during angioplasty. Recently, however, Monge et al.[3] reported excellent acute and long-term surgical results, effectively reducing the RV pressure and providing a freedom from reintervention of 93% at a median follow-up of 5 years.

One proposed surgical approach has consisted of a single-stage, comprehensive repair in the majority of cases, with a novel, two-stage approach in a select, minority of severely unbalanced cases.[10] In the staged repair, hypoplastic and stenotic PA branches in the underperfused lung (usually the left) are repaired first to promote perfusion and growth; the stenoses in the contralateral side are not addressed until the second stage. If both sides are repaired simultaneously in this setting, then improvements in pressure are seen but the flow distribution remains grossly maldistributed. In the past, the choice of single- or multi-staged repair has been based on the preoperative evaluations (computed tomography [CT] angiography, lung perfusion scan [LPS], and cardiac catheterization data), past anecdotal surgical experience and surgeon preference/opinion. A more broadly applicable, patient-specific approach to PPS stenosis in various populations could be beneficial.

Computational fluid dynamics (CFD) has been increasingly used to study cardiovascular diseases associated with the pulmonary circulation including single ventricle defects, tetralogy of Fallot, and pulmonary arterial hypertension.[11–16] Flow simulations allow one to test and validate interventions safely "in silico." Despite numerous studies on the hemodynamics and surgical planning for the single ventricle defects,[17–21] few studies have employed CFD to better understand PPS and evaluate the current approaches.[22] Patients with Alagille syndrome, while not alone in their high incidence of PPS, represent an excellent sample population to refine the use of computational simulation techniques for postintervention prediction. Recently, we proposed an adaptive outflow boundary condition method to improve the estimation of overall pulmonary flow distribution after PPS repair in this population.[22] The purpose of this pilot study is to use recently refined computational simulation in the setting of multiple surgical strategies, to examine the influence of PA reconstruction on hemodynamics in this population.

Modeling hemodynamics in patients with PPS, in this case with Alagille syndrome, but equally applicable to those with Williams and other syndromes, before and after intervention will serve as a stepping stone to ultimately develop a robust surgical planning tool that could be applicable to a broader spectrum of more complex congenital heart defects (eg, pulmonary atresia/ventricular septal defect/major aortopulmonary collateral arteries) treated by similar surgical and transcatheter techniques.[23]

2 | MATERIALS AND METHODS

2.1 | Clinical data acquisition

A protocol for the use of cardiac imaging data for flow simulations was approved by the Stanford University Institutional Review Board. Patients with Alagille syndrome who had undergone PA reconstruction for PPS at Lucile Packard Children's Hospital were identified and those with preoperative cardiac catheterization and CT angiography, and pre- and postoperative LPS were included.

Computed tomography angiography of the chest was performed after administration of iohexol as described previously.[24,25] Standard right heart catheterization was performed as part of routine clinical procedures. Pulmonary artery pressures were measured during routine cardiac catheterization using fluid-filled catheters, and cardiac output was determined using Fick or thermodilution methods as appropriate. To quantify the pulmonary flow distribution, lung images were taken immediately after administration of Tc-99m MAA (microaggregated albumin) and pulmonary perfusion percentages were derived from geometric mean analysis.[26]

2.2 | Model construction and simulation

Three dimensional CT-based preoperative PA models (Figure 1) were constructed using SimVascular (simvascular.org).[27] The main pulmonary artery (MPA) and branch PAs to the subsegmental level were included. The creation of virtual postoperative models was constructed in consultation with the surgeon performing the operation to mirror both potential approaches (ie, 1- vs 2-stage) and anatomic results. Specifically, surgically addressed pulmonary arteries were enlarged and modified to represent the homograft patches utilized during surgical reconstruction.

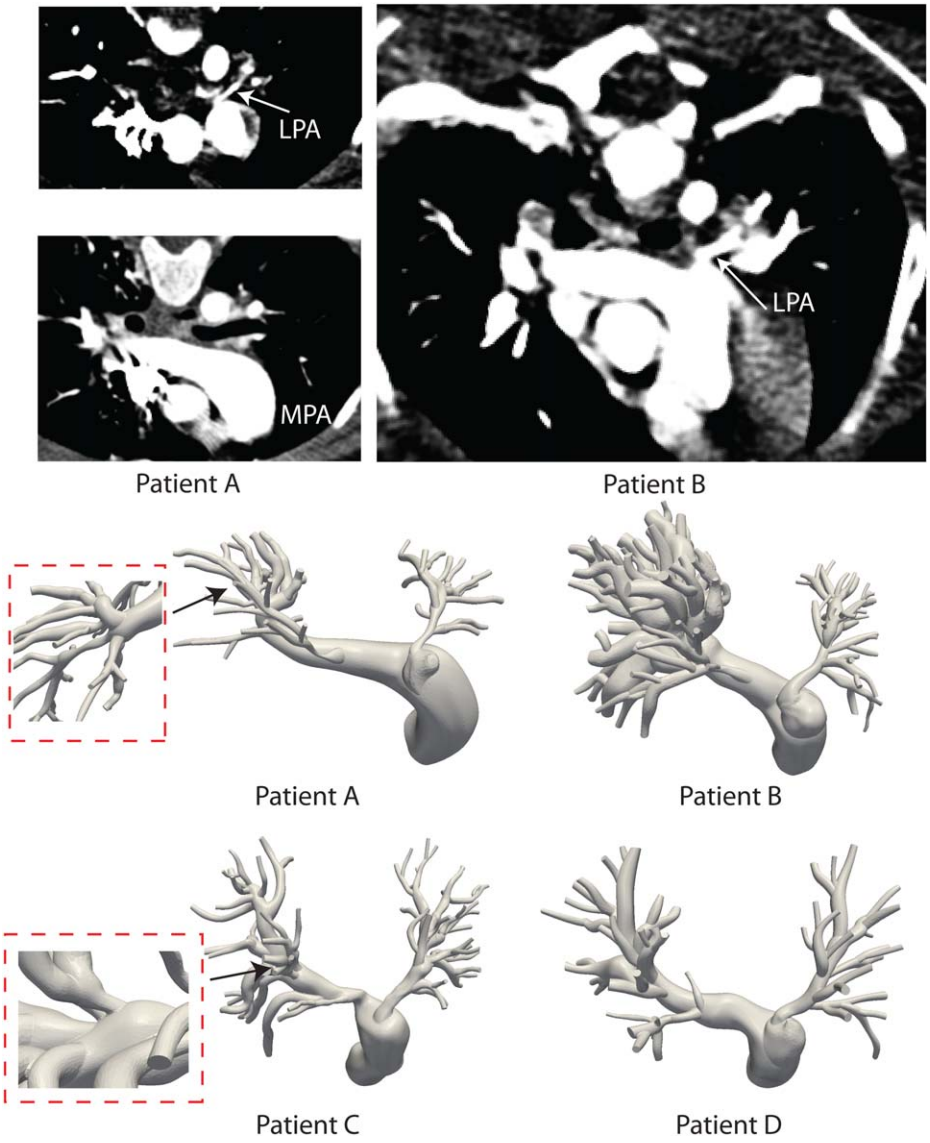

FIGURE 1 Selected CT angiography and complete preoperative models. Central LPA hypoplasia with multiple segmental and subsegmental stenoses is present

In patients undergoing staged repair, it is our practice to perform cardiac catheterization with angiography and then surgical completion approximately 6 months after the first surgery. Cardiac catheterization angiography is used to evaluate interval vessel growth, resulting from the increased flow. Thus, in creating the new baseline preoperative model, accounting for vessel growth prior to the second surgery, the distal branches were enlarged based on the angiographic measurements (Figure 2). To compare whether a staged repair approach provided any real benefit, virtual single-stage models were created by relieving stenoses bilaterally without any enlargement for growth. In 1 patient, a postoperative CT scan was available; this single postoperative model was created from the postoperative CT rather than from angiography.

Blood flow was modeled using three-dimensional Navier–Stokes equations under incompressibility and Newtonian assumptions with density and viscosity values set at 1.06 g/cm^3 and 0.04 g/(cm), respectively. As rigid wall assumptions overestimate systolic pressures,[28,29] we employed a fluid–solid interaction finite element solver to account for arterial compliance.[28] The wall is modeled by linear elastic equations, and equations for wall deformation are coupled to the governing equations of blood flow.[28] The parameters were set as follows: wall density = 1.0 g/cm^3, Poisson's ratio = 0.5, and shear correction parameters = 5/6. The values for the Young's modulus and wall thickness were 2.6–4.2 $\times$ 10^6 dyn/cm^2 and 0.05 cm, respectively. Young's modulus and wall thickness were then manually adjusted for each patient to match cath-derived pressures.

Pulmonary mean flow rates were based on the catheterization-derived values. Inflow waveforms were taken from the study of Tang et al.[30] and scaled iteratively with the Young's modulus for the wall, and outflow boundary conditions to match preoperative PA systolic, diastolic, and mean pressures obtained by catheterization. For outflow boundary conditions, 3-element Windkessel models were employed to

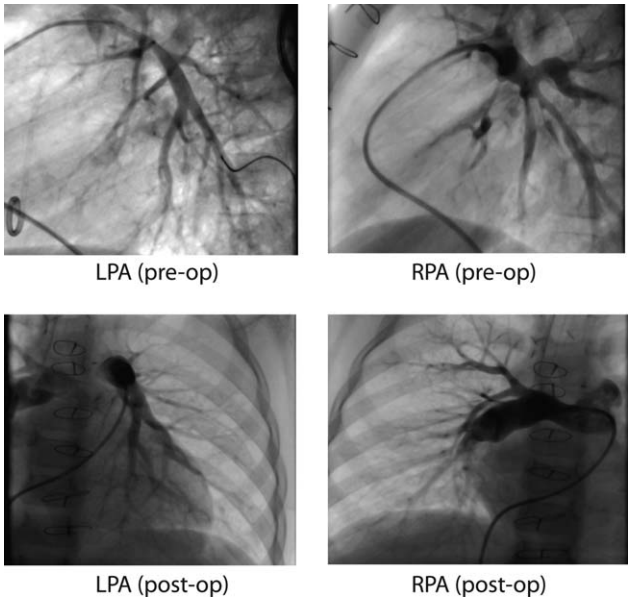

FIGURE 2 Selected pre- and postoperative angiograms of distal PAs in patient A

model distal PAs.[31,32] For each preoperative model, simulations were repeated and resistance parameters adjusted until in vivo PA pressures and flow splits were matched. As distal PAs are modeled by parallel Windkessel models, the total downstream resistance for each lung is approximated by the equation:

$$\frac{1}{R_{r(l)}} = \sum_{i=1}^{n} \frac{1}{RCR_i^{r(l)}} \quad (1)$$

Where $r(l)$ denotes the right pulmonary artery (RPA) (left pulmonary artery, LPA), $R_{r(l)}$ is the total downstream resistance for the RPA (LPA), n is the number of outlets of the RPA (LPA) in the patient-specific model, and $RCR_i^{r(l)}$ is the resistance of the Windkessel model for the *i*th outlet in the RPA (LPA).

To accurately estimate postoperative pulmonary flow splits, an adaptive outflow boundary condition[22] is necessary. This method allows for vessel adaptation (vasodilation) in response to increased blood flow.[33] To model postoperative outflow boundary conditions, a structured tree model proposed by Olufsen et al.[34–36] is used in conjunction with the constant wall shear stress (WSS) assumption to estimate the postoperative resistance. For each outlet, a baseline-structured tree is generated such that the total resistance is equal to the resistance of the Windkessel model used for the preoperative simulations. A simulation is then performed on the virtual postoperative model using the same preoperative boundary conditions. By comparing the flow changes, the segments in the baseline-structured trees will be dilated or constricted to restore the level of WSS in the preoperative stage. A new set of outlet resistances is given by the adapted structured trees and applied to the postoperative model. As immediate postoperative catheterization data are not available, and pulmonary flow distribution is not sensitive to the changes in cardiac output,[22] inflow conditions (ie, pulmonary blood flow/cardiac output) were assumed to be unchanged. Figure 3 shows the major steps from model construction to postoperative hemodynamic modeling.

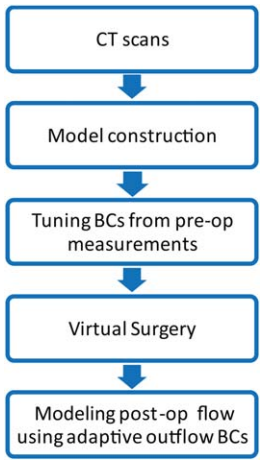

FIGURE 3 Major steps for hemodynamic modeling of patients with PPS undergoing surgical repair

3 | RESULTS

Four patients (male, age range: 0.6–2.9 years) with the necessary pre- and postoperative anatomic and hemodynamic data were identified; their demographics and diagnostic testing results are summarized in Table 1. Figure 1 shows CT images and preoperative models for each patient. As previously described, the "classic" phenotype was present in all 4 patients—long segment LPA hypoplasia with small distal vessel and multiple focal stenoses located at bifurcation and trifurcation points.[25]

Each patient had significant PPS, RV hypertension, and pulmonary flow disparity. Based on the surgeon's preference, patients underwent either a 1-stage (n = 2) or 2-stage (n = 2) repair. Patient A underwent a 2-stage repair: the hypoplastic LPA was reconstructed at the first surgery, and the stenoses in the RPA were addressed 6 months later. The measurements from postoperative angiograms showed that distal LPA branches increased by 46% (Figure 2). Similarly, for patient B the LPA was addressed initially; the patient underwent liver transplantation after stage 1, and the remaining stenoses were addressed 2 years after stage 1. For this patient, postoperative models were created solely for the first stage and for a virtual single stage as no imaging data prior to this patient's second stage were available.

Figure 4 shows the simulation results for pre- and postoperative mean PA pressure. Preoperative simulations for patients A, B, and C were tuned to match existing clinical data, and postoperative models represent the estimation of PA pressure based solely on the computational simulations. In Figure 4, the postoperative model for patient D was created directly from postoperative CT images and pre- and postoperative pressure distribution was given by simulations tuned to match the pre- and postoperative LPS results (73R/27L vs 81R/19L), respectively. Models replicated the clinical measurements (eg, in patient A, the LPA stenosis results in a

TABLE 1 Preoperative demographic and diagnostic data

Patient	Age (y)	BSA (m^2)	RVP (mm Hg)[a]	PAP (mm Hg)	Lung perfusion (R/L%)	Associated conditions
A (1st stage)	2.9	0.58	75/9	71/16 (RPA)	86/14	Granuloma annulare, VSD
A (2nd stage)	3.3	0.64	49/7	47/13 (MPA)	37/63	
B (1st stage)	1.9	0.48	74/11	72/14 (MPA)	80/20	Liver failure, VSD, PAPVR
C	1.8	0.40	75/21	75/24 (MPA)	66/34	Biliary atresia, canalicular cholestasis, liver failure
D	0.7	0.35	47/8	37/10 (RPA)	73/27[b]	Chronic cholestasis

Abbreviations: BSA, body surface area; PAP, pulmonary artery pressure; PAPVR, partial anomalous pulmonary venous return; RVP, right ventricular pressure measured via catheterization; VSD, ventricular septal defect.
[a]RVP is presented as systolic/diastolic pressures and lung perfusion result is shown as right/left split. Patient A underwent staged surgical reconstruction.
[b]LPS performed 6 months before preop.

>30 mm Hg gradient and agrees with the catheterization data), and demonstrate that patching the LPA effectively reduces the gradient and overall PA pressure.

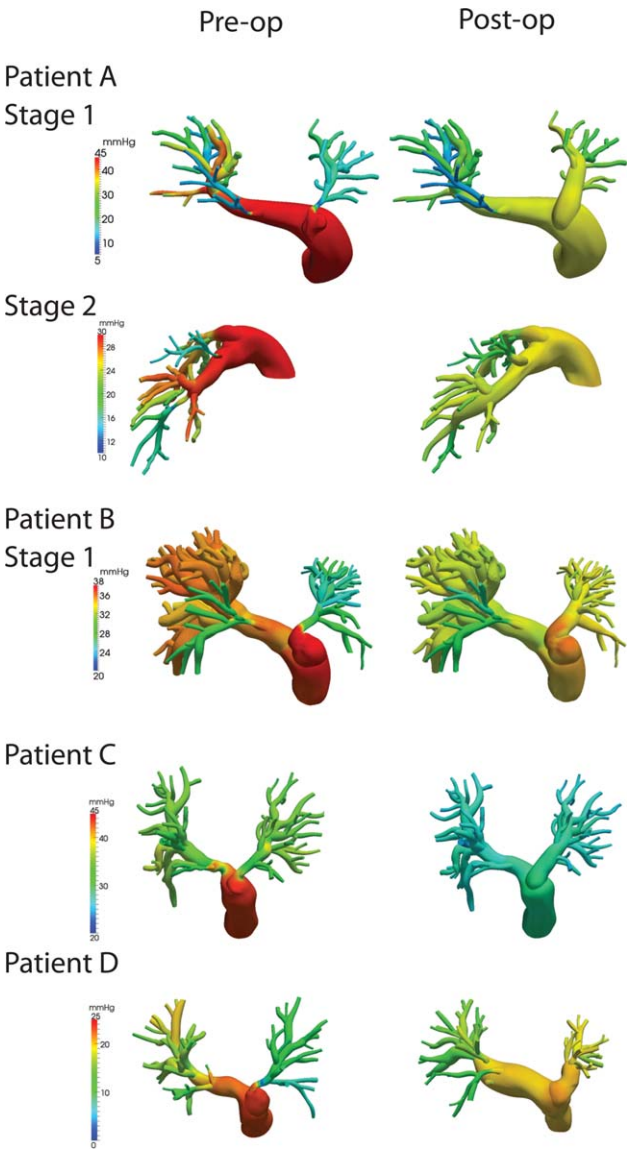

FIGURE 4 Mean pressures in the pre- and postoperative models for patients A, B, C, and D

A comparison of postoperative LPSs and simulation-derived pulmonary flow distribution is shown in Figure 5. In patients A, B, and C, excellent agreement was found between simulations and in vivo measurements. The simulated single-stage (instead of the actual 2-stage) repair in patient A found that the 1-stage repair would result in a less balanced flow distribution (68R/32L) than the 48R/52L, resulting from the actual 2-stage repair, suggesting a potential benefit to the 2-stage repair in this patient. In patient B, initial LPA-plasty resulted in a flow split of 63R/37L and 54R/46L for 1 and 14 weeks after repair, respectively; in brief, 2 years later, after addressing the RPA, 65R/35L was the final blood flow distribution. The simulated single-stage repair resulted in a flow split of 68R/32L. Given the length of time between first and second stages, it is unclear whether the 54R/46L split seen shortly after stage 1 was still present just prior to stage 2 but the simulation suggests that a 1-stage repair in this patient may have yielded similar final results, and demonstrating the potential usefulness of this technique in surgical planning.

Finally, the immediate postoperative LPS in patient D demonstrated less balanced blood flow distribution (81R/19L) than the preoperative scan (73R/27L). The simulation, however, reported a postoperative flow split of 65R/35L if the preoperative boundary conditions were kept unchanged. Postoperative CT imaging was performed and did not demonstrate any new stenoses, and showed an enlarged and widely patent ostium. Thus, it was believed by the clinical team that the downstream resistance in the left lung had increased during the 6-month period between the lung scan and the surgery, leading to a greater flow disparity than the 73R/27L measured 6 months earlier. Concerned that the preoperative LPS for patient D was therefore inaccurate, we ran an additional simulation using the postoperative stage as the baseline, and applied adaptive outflow boundary conditions "backward" to estimate what the immediate *preoperative* hemodynamics would have to be to obtain the lung scan results. If the assumption that the LPS was outdated is correct, then the simulation estimated the true preoperative flow split would have been closer to 84R/16L, not that dissimilar to the prior lung scan but different enough to effect the simulation results. Two years later, a repeat LPS was 68R/32L, showing some interval improvement, but 5 years after that remains 67R/33L (Figure 5).

Downstream (ie, small vessel resistance) resistance in the pre- and postoperative stages was calculated using Equation (1) and shown in

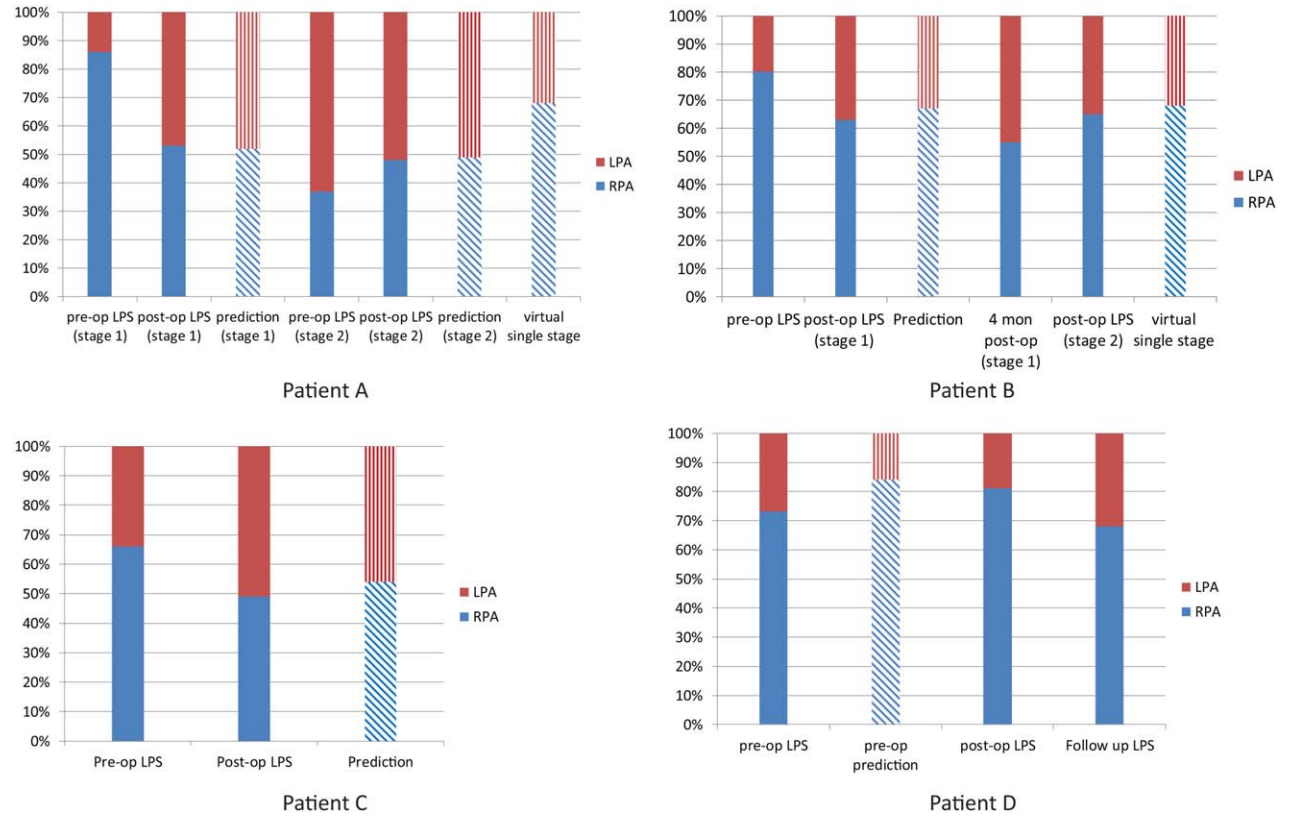

FIGURE 5 Postoperative lung perfusion scans and simulation-derived pulmonary flow distribution. The term of prediction is used in the context of modeling postoperative hemodynamics without using any postoperative data. For patient D, as the preoperative LPS was performed 6 months before repair, immediate preoperative pulmonary flow distribution was estimated by simulations

Figure 6. As comparison of the relative magnitude, the resistance generated by the diffuse proximal LPA stenosis is also shown in Figure 6. Once removed, the proximal stenosis has negligible resistance (Figure 4) and is thus not presented. The downstream LPA resistance dropped significantly, whereas the downstream RPA resistance increased moderately in patients A, B, and C after the LPA stenosis was repaired. In each case, as seen physiologically, increased flow led to decreased resistance and vice versa. Specifically, as the clinical postoperative flow split for patient D is worse than the preoperative value (73R/27L), and flow to the LPA decreased, it is not surprising that our results show that increased downstream resistance for the LPA resulted in further skewed flow distribution. The LPA stenosis represents significant resistance, comparable to the downstream resistance, and as such, was the leading factor in the flow disparity in patients A, C, and D.

4 | DISCUSSION

In this study, we used computational simulation methods to estimate patient-specific postoperative hemodynamics in 4 patients with Alagille syndrome and PPSs. By incorporating adaptive outflow boundary conditions, we obtained satisfactory agreement with the clinical diagnostic testing data for relative blood flow distribution and PA pressures based solely on the preoperative data. This advanced modeling of the pulmonary vascular tree represents an important step toward the ongoing refinement of computational techniques to ultimately accurately represent the pre- and posttreatment states of both simple and complex congenital heart disease patients.

In this population, a single, comprehensive repair of proximal and distal left and RPA stenoses is the procedure of choice as this can successfully reduce the PA pressures to near-normal or normal levels. In selected patients, however, with particularly discrepant right/left pulmonary blood flow distribution resulting from one side (usually the left) being far more hypoplastic and underdeveloped, a single-stage repair will reduce the pressure but not improve the relative perfusion. It has been suggested that a staged approach will allow the previously underperfused lung (usually the left lung) to grow over time as a result of increased blood flow mitigated by leaving stenoses on the contralateral side to "force" flow to the newly repaired lung. In animal studies, greatly skewed blood flow distribution (~80R/20L) was shown to result in impaired lung and vascular growth.[37] Although no definitive guidelines exist, expert opinion suggests that surgical or transcatheter attempts to increase flow to an affected lung in the setting of stenosis should be considered when flow to the effected lung is <30%.

Not surprisingly, the single-stage repair is most common at our center. In a small subset of patients, however, it was noted that postoperative pulmonary flow distribution remained quite skewed and the interest in a 2-stage approach for these unique patients evolved, and successful reports published.[3] Surgical approaches to the first of the 2 stages to promote growth have included repairing the severe proximal stenosis alone, creating a discontinuity and placing a systemic to

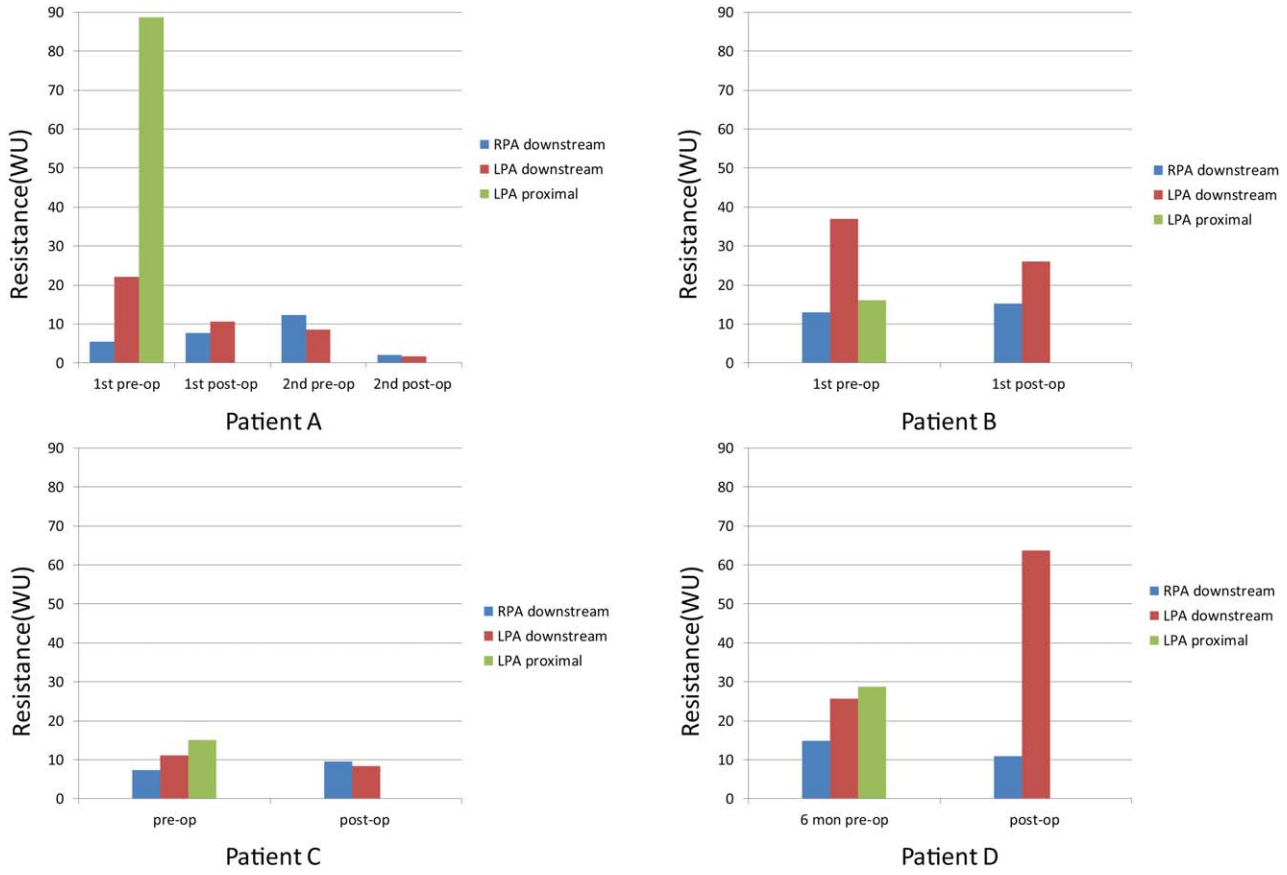

FIGURE 6 Downstream pulmonary resistance and LPA ostial resistance for the pre- and postoperative stages. Downstream resistance is derived from the outflow boundary conditions that match pre- and postoperative pulmonary flow distribution using Equation (1). The ostial LPA resistance is calculated using the pressure drop and flow across the stenosis

pulmonary shunt to the greatly affected side, or repair of the severe proximal stenosis with banding of the contralateral side. However, the hemodynamic superiority of staged repair has not been examined previously, and in this study, we performed flow simulations to compare the hemodynamic performance of single- and two-stage repairs in a few selected patients who underwent the staged procedure.

Postoperative LPSs demonstrated a well-balanced final pulmonary circulation in patient A who underwent staged repair; simulations suggest that relative flow distribution for a single-stage repair would be less balanced than that seen with a 2-stage repair. In patient B, however, whose preoperative pulmonary flow split was also highly skewed, the discrete ostial stenosis in the RPA did not provide enough "resistance" to achieve a 50/50 flow split immediately after the LPA was reconstructed. It is therefore not surprising a virtual single-stage repair resulted in a similar flow split. This would suggest that a single-stage repair would have achieved similar results to the 2-stage repair performed.

Given that the "eyeball" test and lung scan data yield, not surprisingly, variable results, it is important to have tools that allow providers to evaluate the preoperative state, that is the resistance created by the stenoses and downstream vascular beds separately, to determine an optimal surgical strategy. Figure 7 shows the principle of staged repair qualitatively. Briefly, the RPA (and LPA) can be approximated by 2 resistors R_{r1} (R_{l1}) and R_{r2} (R_{l2}) in series representing the "large" (ie, segmental and more proximal) and "small" (subsegmental and microvasculature) vessels, respectively. If the small vessel resistance (R_{r2} and R_{l2}) is similar (ie, the pulmonary vascular resistance is low, and the subsegments are similarly sized), relieving all stenoses in the PAs at the same time may restore a normal flow split. Staged repair is indicated when there is a large difference in distal resistance (R_{r2} and R_{l2}). The staged strategy leverages the resistance created by the contralateral stenoses (eg, R_{r1}) to balance the inequality in the downstream resistance (R_{r2} and R_{l2}). If the stenoses in the RPA and LPA were relieved in the same stage, then the flow to the LPA may be great enough perfusion to promote growth. When the proximal stenoses are less severe and pulmonary flow disparity is more influenced by downstream resistance R_{r2} and R_{l2} as shown in Figure 7B, unsatisfactory flow distribution persists after bilateral stenoses are relieved in a single-stage surgery. The patients present with a wide variety of anatomic and physiologic (ie, pulmonary flow distribution) variability. The distal resistance, the key component in postoperative pulmonary blood flow distribution, however, is not easily calculated using existing clinical methods. Computational simulations may offer an opportunity to refine our diagnostic and therapeutic approach to these complex patients and play a role in identifying an optimal strategy for complex cases.

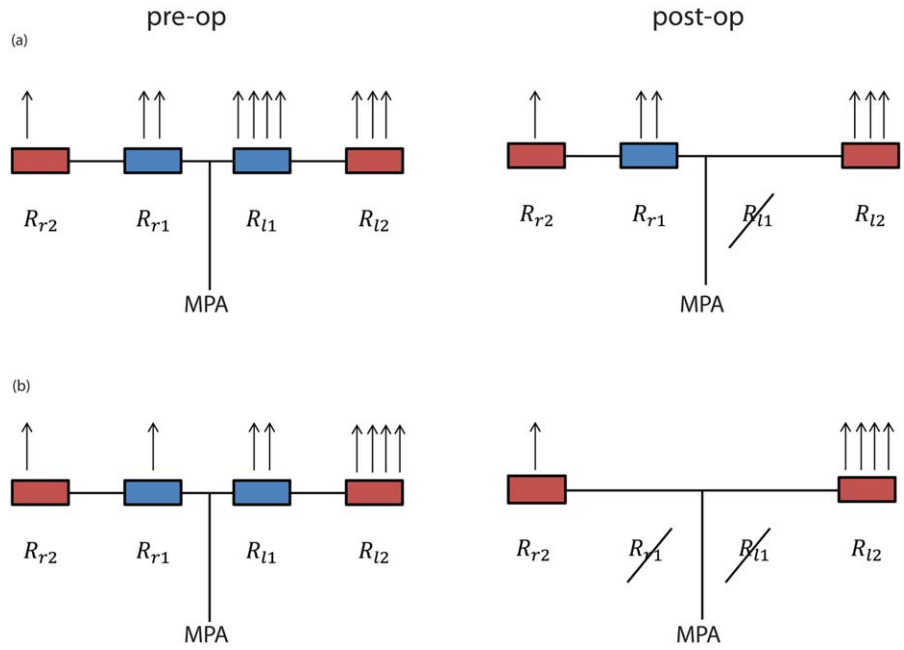

FIGURE 7 Schematic diagrams for two scenarios of PPS repair. The resistance caused by proximal stenosis and distal vasculature in the RPA (LPA) is represented by R_{r1} (R_{l1}) and R_{r2} (R_{l1}), respectively. The number of arrows on each resistor represents the impact of resistance. A, High resistance for R_{l1} indicates an extremely tight proximal LPA. If the stenoses in the RPA (R_{r1}) are kept and the LPA stenosis (R_{l1}) is relieved, the overall resistance for each lung is balanced. B, Overall resistance for the RPA and LPA is highly unequal but the stenoses in the proximal LPA and RPA are less severe. Skewed pulmonary flow distribution can be created by relieving stenoses in the RPA and LPA (R_{r1} and R_{l1}) in the same stage

5 | LIMITATIONS

Nonpatient-specific flow waveforms were used in simulations, and inflow conditions were assumed unchanged between the preoperative and immediately postoperative stages. In future studies, a lumped parameter heart model could be incorporated to model postoperative inflow. The postoperative models that were virtually reconstructed with the assistance of the surgeon performing the procedure (rather than with postoperative CT data) may affect the accuracy of the postoperative anatomy. Preoperative measurements are not available for patient B's second surgical repair. With recent advances in 4DMRI techniques,[38] time-dependent velocity vectors as well as anatomy over an imaging volume can be obtained with significantly reduced scan time (~20 minutes). Thus, 4DMRI with catheterization may provide more physiological data than current CT/LPS/catheterization evaluations. Future studies should collect paired pre- and postoperative 4DMRI/catheterization data to validate simulation-based predictions including virtual postoperative geometry, pulmonary flow distribution, and pressure reductions.

6 | CONCLUSIONS

We have performed CFD flow simulations to study the hemodynamics in pre- and postoperative patients with Alagille syndrome with complex PPS. In these patients, PPS can play an important role in RV hypertension and pulmonary flow disparity. Using new techniques, we obtained good agreement with in vivo measurements of relative blood flow distribution and PA pressures based solely on preoperative data. Adaptive outflow boundary conditions should be incorporated to take into account downstream pulmonary vasoreactivity in response to surgical repair and changes in flow. Although single-stage repair results in satisfactory outcomes in the overwhelming majority of cases, careful surgical planning is needed for patients with complex PPS and widely discrepant blood flow distribution. Computer simulation may provide a useful adjunct to other clinical diagnostic methods when considering surgical or transcatheter interventions in patients with PPS.

ACKNOWLEDGMENTS

The authors thank Elisa McCarthy, Keeley Phillips, and Renee Rodriguez, MD, for their assistance with IRB consent and clinical data collection. This study is supported by the Vera Moulton Wall Center for Pulmonary Vascular Disease at Stanford and the France-Stanford Center for Interdisciplinary Studies.

CONFLICT OF INTEREST

None.

AUTHOR CONTRIBUTION

All authors read and approved the final version of the manuscript.
Study design: Jeffrey Feinstein
Methodology: Weiguang Yang, Irene Vignon-Clementel, Jeffrey Feinstein

Clinical data acquisition: Jeffrey Feinstein, Frank Hanley, Frandics Chan

Numerical simulations: Weiguang Yang

Computational resource: Alison Marsden

Data analysis/interpretation: Weiguang Yang, Jeffrey Feinstein, Irene Vignon-Clementel, Alison Marsden, Frank Hanley

Drafting article: Weiguang Yang

Critical revision of article: Jeffrey Feinstein, Weiguang Yang, Irene Vignon-Clementel

Approval of article: Jeffrey Feinstein, Irene Vignon-Clementel

ORCID

Weiguang Yang PhD http://orcid.org/0000-0003-3324-4346

REFERENCES

[1] Krantz ID, Piccoli DA, Spinner NB. Alagille syndrome. *J Med Genet*. 1997;34(2):152–157.

[2] Turnpenny PD, Ellard S. Alagille syndrome: pathogenesis, diagnosis and management. *Eur J Hum Genet EJHG*. 2012;20(3):251–257.

[3] Monge MC, Mainwaring RD, Sheikh AY, Punn R, Reddy VM, Hanley FL. Surgical reconstruction of peripheral pulmonary artery stenosis in Williams and Alagille syndromes. *J Thorac Cardiovasc Surg*. 2013;145(2):476–481.

[4] Cunningham JW, McElhinney DB, Gauvreau K, Bergersen L, Lacro RV, Marshall AC. Outcomes after primary transcatheter therapy in infants and young children with severe bilateral peripheral pulmonary artery stenosis. *Circ Cardiovasc Interv*. 2013;6(4):460–467.

[5] Kamath BM, Spinner NB, Emerick KM, Chudley AE, Booth C, Piccoli DA. Vascular anomalies in Alagille syndrome: a significant cause of morbidity and mortality. *Circulation*. 2004;109(11):1354–1358.

[6] Tzakis AG, Reyes J, Tepetes K, Tzoracoleftherakis V, Todo S, Starzl TE. Liver transplantation for Alagille's syndrome. *Arch Surg Chic Ill 1960*. 1993;128(3):337–339.

[7] Marino IR, ChapChap P, Esquivel CO, et al. Liver transplantation for arteriohepatic dysplasia (Alagille's syndrome). *Transpl Int*. 1992;5(2):61–64.

[8] Trivedi KR, Benson LN. Interventional strategies in the management of peripheral pulmonary artery stenosis. *J Intervent Cardiol*. 2003;16(2):171–188.

[9] Trant CA Jr, O'Laughlin MP, Ungerleider RM, Garson A Jr. Cost-effectiveness analysis of stents, balloon angioplasty, and surgery for the treatment of branch pulmonary artery stenosis. *Pediatr Cardiol*. 1997;18(5):339–344.

[10] Mainwaring RD, Ibrahimiye AN, Hanley FL. Surgical technique for repair of peripheral pulmonary artery stenosis and other complex peripheral reconstructions. *Ann Thorac Surg*. 2016;102(2):e181–e183.

[11] Vignon-Clementel IE, Marsden AL, Feinstein JA. A primer on computational simulation in congenital heart disease for the clinician. *Prog Pediatr Cardiol*. 2010;30(1–2):3–13.

[12] Pennati G, Corsini C, Hsia T-Y, Migliavacca F. Computational fluid dynamics models and congenital heart diseases. *Front Pediatr [Internet]*. 2013;1:4. February 26 [cited 2015 Apr 30]; Available from: http://www.ncbi.nlm.nih.gov/pmc/articles/PMC3882907/

[13] Tang BT, Pickard SS, Chan FP, Tsao PS, Taylor CA, Feinstein JA. Wall shear stress is decreased in the pulmonary arteries of patients with pulmonary arterial hypertension: an image-based, computational fluid dynamics study. *Pulm Circ*. 2012;2(4):470–476.

[14] Kheyfets VO, O'Dell W, Smith T, Reilly JJ, Finol EA. Considerations for numerical modeling of the pulmonary circulation—a review with a focus on pulmonary hypertension. *J Biomech Eng*. 2013;135(6):0610111–06101115.

[15] Das A, Banerjee RK, Gottliebson WM. Right ventricular inefficiency in repaired tetralogy of Fallot: proof of concept for energy calculations from cardiac MRI data. *Ann Biomed Eng*. 2010;38(12):3674–3687.

[16] Caiazzo A, Guibert R, Boudjemline Y, Vignon-Clementel IE. Blood flow simulations for the design of stented valve reducer in enlarged ventricular outflow tracts. *Cardiovasc Eng Technol*. 2015;6(4):485–500.

[17] Dubini G, Leval MR, de Pietrabissa R, Montevecchi FM, Fumero R. A numerical fluid mechanical study of repaired congenital heart defects: application to the total cavopulmonary connection. *J Biomech*. 1996;29(1):111–121.

[18] Bove EL, de Leval MR, Migliavacca F, Guadagni G, Dubini G. Computational fluid dynamics in the evaluation of hemodynamic performance of cavopulmonary connections after the Norwood procedure for hypoplastic left heart syndrome. *J Thorac Cardiovasc Surg*. 2003;126(4):1040–1047.

[19] Marsden AL, Bernstein AJ, Reddy VM, et al. Evaluation of a novel Y-shaped extracardiac Fontan baffle using computational fluid dynamics. *J Thorac Cardiovasc Surg*. 2009;137(2):394–403.e2.

[20] Yang W, Chan FP, Reddy VM, Marsden AL, Feinstein JA. Flow simulations and validation for the first cohort of patients undergoing the Y-graft Fontan procedure. *J Thorac Cardiovasc Surg*. 2015;149(1):247–255.

[21] Pekkan K, White B, Kanter K, et al. Patient-specific surgical planning and hemodynamic computational fluid dynamics optimization through free-form haptic anatomy editing tool (SURGEM). *Med Biol Eng Comput*. 2008;46(11):1139–1152.

[22] Yang W, Feinstein JA, Vignon-Clementel IE. Adaptive outflow boundary conditions improve post-operative predictions after repair of peripheral pulmonary artery stenosis. *Biomech Model Mechanobiol*. 2016; 15(5):1345–1353.

[23] Reddy VM, Liddicoat JR, Hanley FL. Midline one-stage complete unifocalization and repair of pulmonary atresia with ventricular septal defect and major aortopulmonary collaterals. *J Thorac Cardiovasc Surg*. 1995;109(5):832–844. discussion 844–5.

[24] Chan FP, Hanneman K. Computed tomography and magnetic resonance imaging in neonates with congenital cardiovascular disease. *Semin Ultrasound CT MR*. 2015;36(2):146–160.

[25] Rodriguez RM, Feinstein JA, Chan FP. CT-defined phenotype of pulmonary artery stenoses in Alagille syndrome. *Pediatr Radiol*. 2016;46(8):1120–1127.

[26] Cheng CP, Taur AS, Lee GS, Goris ML, Feinstein JA. Relative lung perfusion distribution in normal lung scans: observation and clinical implications. *Congenit Heart Dis*. 2006;1(5):210–216.

[27] Schmidt JP, Delp SL, Sherman MA, Taylor CA, Pande VS, Altman RB. The Simbios National Center: Systems Biology in Motion. *Proc IEEE Inst Electr Electron Eng*. 2008;96(8):1266–1280.

[28] Figueroa CA, Vignon-Clementel IE, Jansen KE, Hughes TJR, Taylor CA. A coupled momentum method for modeling blood flow in three-dimensional deformable arteries. *Comput Methods Appl Mech Eng*. 2006;195(41–43):5685–5706.

[29] Konala BC, Das A, Banerjee RK. Influence of arterial wall-stenosis compliance on the coronary diagnostic parameters. *J Biomech*. 2011;44(5):842–847.

[30] Tang BT, Fonte TA, Chan FP, Tsao PS, Feinstein JA, Taylor CA. Three-dimensional hemodynamics in the human pulmonary arteries under resting and exercise conditions. *Ann Biomed Eng*. 2011;39(1):347–358.

[31] Spilker RL, Feinstein JA, Parker DW, Reddy VM, Taylor CA. Morphometry-based impedance boundary conditions for patient-specific modeling of blood flow in pulmonary arteries. *Ann Biomed Eng*. 2007;35(4):546–549.

[32] Troianowski G, Taylor CA, Feinstein JA, Vignon-Clementel I. Three-dimensional simulations in Glenn patients: clinically based boundary conditions, hemodynamic results and sensitivity to input data. *J Biomech Eng*. 2011;133(11):111006.

[33] Kamiya A, Togawa T. Adaptive regulation of wall shear stress to flow change in the canine carotid artery. *Am J Physiol*. 1980;239(1):H14–H21.

[34] Olufsen MS. Structured tree outflow condition for blood flow in larger systemic arteries. *Am J Physiol*. 1999;276(1 Pt 2):H257–H268.

[35] Olufsen MS, Peskin CS, Kim WY, Pedersen EM, Nadim A, Larsen J. Numerical simulation and experimental validation of blood flow in arteries with structured-tree outflow conditions. *Ann Biomed Eng*. 2000;28(11):1281–1299.

[36] Olufsen MS, Hill NA, Vaughan GDA, Sainsbury C, Johnson M. Rarefaction and blood pressure in systemic and pulmonary arteries. *J Fluid Mech*. 2012;705:280–305.

[37] Razavi H, Stewart SE, Xu C, et al. Chronic effects of pulmonary artery stenosis on hemodynamic and structural development of the lungs. *Am J Physiol Lung Cell Mol Physiol*. 2013;304(1):L17–L28.

[38] Vasanawala SS, Hanneman K, Alley MT, Hsiao A. Congenital heart disease assessment with 4D flow MRI. *J Magn Reson Imaging JMRI*. 2015;42(4):870–886.

How to cite this article: Yang W, Hanley FL, Chan FP, Marsden AL, Vignon-Clementel IE, Feinstein JA. Computational simulation of postoperative pulmonary flow distribution in Alagille patients with peripheral pulmonary artery stenosis. *Congenital Heart Disease*. 2018;13:241–250. https://doi.org/10.1111/chd.12556